Central European Journal of Energetic Materials, **2015**, *12*(4), 799-815
ISSN 1733-7178
e-ISSN 2353-1843

Foci for Determining the Insensitivity Features of Nanometer RDX: Nanoscale Particle Size and Moderate Thermal Reactivity

Yi WANG [1,*], Xiaolan SONG [2], Dan SONG [3], Jun ZHANG [2, 4], Kenpeng SONG [2]

[1] *School of Materials Science and Engineering, North University of China, Taiyuan, China*
[2] *School of Chemical Engineering and Environment, North University of China, Taiyuan, China*
[3] *China Ordnance Institute of Science and Technology, Beijing, China*
[4] *Hubei Space Sanjiang Honglin Detection and Control Co. Ltd, Hubei Xiaogan, China*
[*] *E-mail: wangyi528528@aliyun.com*

Abstract: In this paper, the reasons why nanometer RDX showed lower sensitivity than micro RDX is discussed. Herein we supposed two factors affect the sensitivity of nanometer RDX. Firstly, according detonation physics models, a nanometer particle size results in small hot spots and a high critical temperature. These features suggested high safety for nanometer RDX based on the hot spot theory. A further factor is the thermal reactivity of nanometer RDX, which considerably affects the safety of nanometer energetic materials. Employing the Kinetic Compensation Effect, we calculated the kinetic parameters of micro and nanometer RDX. The results indicated that there was no obvious distinction between the activation energies of micro and nanometer RDX, which implies almost the same reactivity of micro and nanometer RDX. Incorporating the results of small hot spots, high critical temperature, and the unchanged reactivity of micro and nanometer RDX, we concluded that nanometer RDX should exhibit low sensitivity as an intrinsic feature.

Keywords: nanometer RDX, sensitivities, reactivity, hot spots, kinetics

1 Introduction

Cyclotrimethylene trinitramine (RDX) is the most important explosive used in various munitions, such as main charges, booster explosives, solid propellants *etc*. Its performance almost exceeds that of TNT; but then, it has a fatal disadvantage restricting the practical application of this nitramine, *i.e*. the safety of RDX is considerably lower than that of TNT. The most direct method for improving safety is surface coating. Wax, fluoro-rubber, HTPB, even TNT have been used as the coating materials to lower the sensitivity of RDX [1-3]. However, the added layers also obviously decreased the energy performance of the explosive. Another method is to ameliorate the crystalline qualities of the explosive, namely to elevate the safety level by modifying the properties of the explosive itself. Usually, the particle density of a coarse explosive is lower than its theoretical value, because many inclusions (air and solution) remain within the crystals of the explosive [4-6]. These hetero materials adversely affect the shock sensitivity of the explosive particles. In addition to inclusions, crystal defects (internal), stress, and particle shape also affect the sensitivity of explosives. Some explosive particles, which obtained via crystallization or recrystallization processes, may contain few defects (such as tiny pores and voids) in their crystals [7, 8].

In fact, besides the factors mentioned above, there is another important property which can potentially influence the shock sensitivity of explosives, *viz*. particle size and size distribution. In previous studies, we tried probing the effect of particle size on the mechanical sensitivity of RDX and HMX [9, 10]. Czerski and Proud studied the relationship between the granular morphology of nitramines and their shock sensitivity [11]. Their experimental data illustrated that the shock sensitivity of nitramine particles was determined by their surface smoothness rather than by their particle size. The critical gap of an HMX sample with mean size 237 μm is even smaller than the value of a sample with mean size 16 μm; no regular tendency dominated the dependence of shock sensitivity on particle size. This was ascribed to the creation mechanism of hot spots (*i.e.* the viscoplastic deformation theory). The theory is very complex, inasmuch as many parameters of the explosive charge are concerned, such as density, pore size, thermal conductivity, and viscosity *etc*. [12-14]. When the particle size is small enough, the micron morphology of explosive particles cannot significantly affect the creation of viscoplastic work. In this case, the very important factor is pore size. If the pore size is lower than the critical size, initiating a detonation in the explosive charge is difficult. The pore size is determined by the explosive's particle size. If the particle size is lower than the submicron (even nanometer) scale, the size of the majority of pores may be smaller than the critical size.

Therefore, it seems that decreasing the particle size is a very promising method for increasing the safety level of explosives. In fact, this method does not apply to some energetic materials unless a certain precondition is met.

This precondition is the steady kinetic characteristics. In any shock sensitivity test or mechanical sensitivity test, the detonation events are attributed to the creation of hot spots, *i.e*. the explosives are ignited by heat. Therefore, the tendency for thermal decomposition significantly influences the sensitivity of explosives. In respect of nitramines, the rate-limiting step of thermolysis is activation of the explosive molecules, and the activation should be almost independent of changes in the specific surface area. As a counter-example, ammonium perchlorate (AP) shows a different characteristic of thermal decomposition. Its "activation" process is proton transfer, *i.e*. the protons in NH_4^+ transfer to ClO_4^- to produce NH_3 and $HClO_4$ ($NH_4^+ + ClO_4^- \rightleftharpoons NH_3(a) + HClO_4(a) \rightleftharpoons NH_3(g) + HClO_4(g)$); however the rate-limiting step is the oxidization of $NH_3(a)$ by $HClO_4(a)$ ($NH_3(a)$ and $HClO_4(a)$ mean the ammonia and perchloric acid which are in adsorbed layer on the surface of AP) [15-17]. This step would be obviously promoted by increasing the specific surface area. Accordingly, the sensitivity of AP increases as its particle size is reduced.

We have here described the fabrication of nanometer RDX and discussed the influences of activation energy and particle size on mechanical and shock sensitivities.

2 Experimental

The micro RDX was comminuted to tiny particles by superfine milling. The specific method of fabricating nanometer RDX is described in [18]. The particle size and size distribution were measured with a laser particle sizer, Master Sizer Instrument. The morphology was observed with a transmission electron microscope (TEM, JEOL JEM-200CX) and an S-4800 field-emission scanning electron microscope (SEM, Hitachi, S4800). The phases of the samples were investigated with an X-ray diffractometer (XRD, Bruker Advance D8), using Cu Kα radiation at 40 kV and 30 mA. The purity of the comminuted samples was characterized by X-ray photoelectron spectroscopy (XPS), PHI5000 Versa-Probe (ULVAC-PHI). Differential scanning calorimetry (DSC) and thermogravimetry (TG) were performed on a TA Model Q600 TG/DSC simultaneous thermal analyzer. The impact test, friction test, and small scale gap test were used to investigate the shock sensitivity of the RDX samples [18, 19].

3 Results

3.1 Size and morphological analysis

The particle size distribution (PSD) profiles of micro and nanometer RDX are presented in Figure 1. The difference between the two distributions was very distinct. For micro RDX, the d_{50} and d_{90} were 84 and 182 μm respectively; after milling, the d_{50} and d_{90} had decreased to 0.27 and 0.5 μm respectively; nanometer RDX shows a narrow size distribution. Because of the huge surface energy, the nanometer RDX particles may agglomerate in the PSD test. Moreover, the resolution of the PSD instrument is more than 0.05 μm. Thus, the measured d_{50} and d_{90} are more than 100 nm. The reason why the size of some particles is >100 nm was also discussed in [18]. TEM and SEM analysis remedied this flaw. In the images (Figure 2), RDX nanoparticles are clearly observed. Most of the pulverized RDX particles are nanosized (<100 nm).

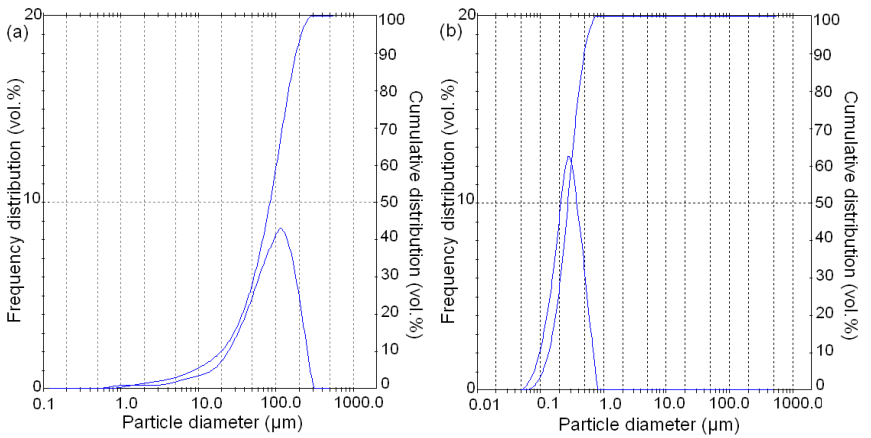

Figure 1. Particle size distribution of: (left) micro RDX; (right) nanometer RDX.

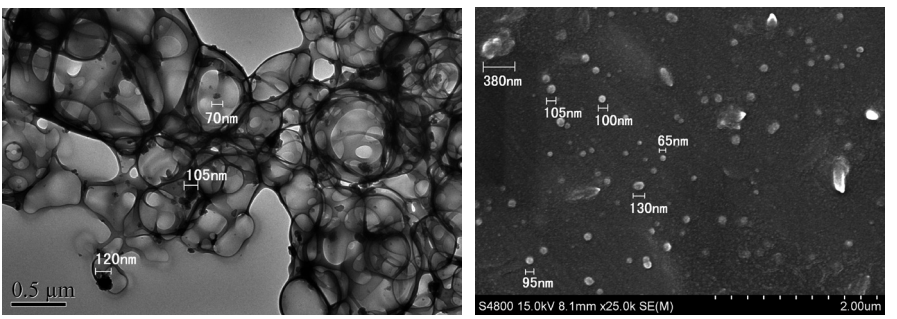

Figure 2. TEM (left) and SEM (right) images RDX nanocrystals.

3.2 Structure analysis

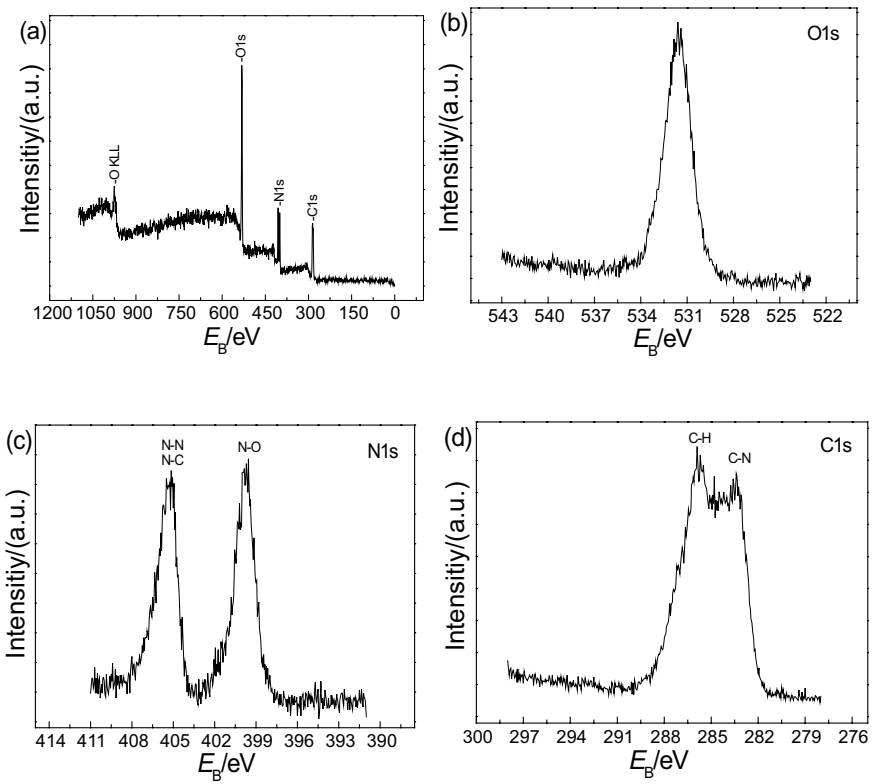

Figure 3. XPS spectra of RDX nanocrystals: (a) the whole spectrum; (b) spectrum of O element; (c) spectrum of N element; (d) spectrum of C element.

The purity of the milled samples was confirmed by XPS and XRD analysis. For both micro-RDX and nanometer RDX, it was demonstrated that only N−O_2, N−N, N−NO_2, and C−H groups exist in the explosive molecules. The XPS spectra of the studied nanoexplosives are illustrated in Figure 3. In both spectra, there are peaks associated with O1s, C1s, and N1s. The O1s peak allows the effect that the nitrate nitrogen has on the electron excitation of O1s to be determined. The C1s peak illustrates the influence that the hydrogen atoms in the CH_2 group and the ammonia nitrogen have on the electron excitation of C1s. The excitation of the N1s electron results in two peaks that represent ammonia nitrogen and nitrate nitrogen respectively. The XRD pattern of nanometer RDX is almost the same as that of micro RDX.

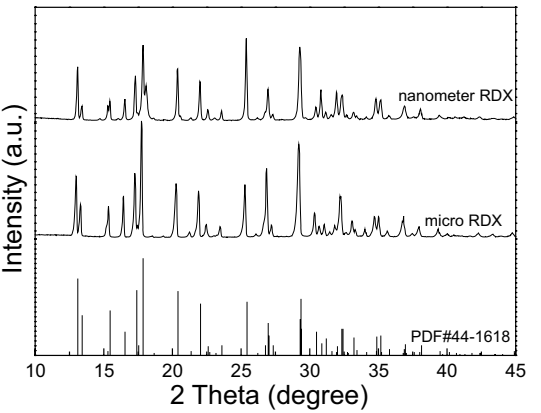

Figure 4. XRD patterns of micro and nanometer RDX crystals.

4 Discussion

This paper is based on results described in Ref. [18]. Therein, the mechanical and shock sensitivities were tested by the impact test, the friction test and the Small Scale Gap Test. Compared with micro RDX, nanometer RDX presented much lower sensitivities. In particular the shock sensitivity of nanometer RDX was lowered by 44.8% compared to the sensitivity of micro RDX.

Table 1. Mechanical and shock sensitivities of raw and nanometer RDX [18]

RDX	Impact sensitivity		Friction sensitivity		Shock sensitivity
	H_{50}, [cm]	S_{dev}	P, [%]	S_{dev}	T_{SSGT}, [mm]
Micro	46.08	4.774	74.00	6.000	14.12
Nanometer	62.75	5.767	59.33	5.033	7.80

We will here discuss in detail why the nanometer nitramine exhibits a higher degree of safety. As illustrated in Figure 5, there are many pores and voids located in an explosive charge. When the charge is subjected to shock stimuli, the pores and voids will be compressed to form "hot spots". The formed hot spots will heat the adjacent explosive and cause parts of them to decompose. However, if the size of the hot spots are not large enough (*i.e.* do not reach the critical size), the heat contribution will not be sufficient to make the decomposition self-sustained. In Moulard's opinion, the usual hot spot models for shock to detonation transition agrees with a two step process [20]. The first step is the hot-spot ignition. This is the limiting step for shock loading of large duration and low shock pressure. The

second step is the chemical reaction growth. This is the limiting step for shock loading of small duration and high shock pressure. Therefore, the differences in pore size and the discrepancy of thermal decomposition properties between nanometer and micron RDX particles, becomes very significant for interpreting why nanometer RDX shows low sensitivities.

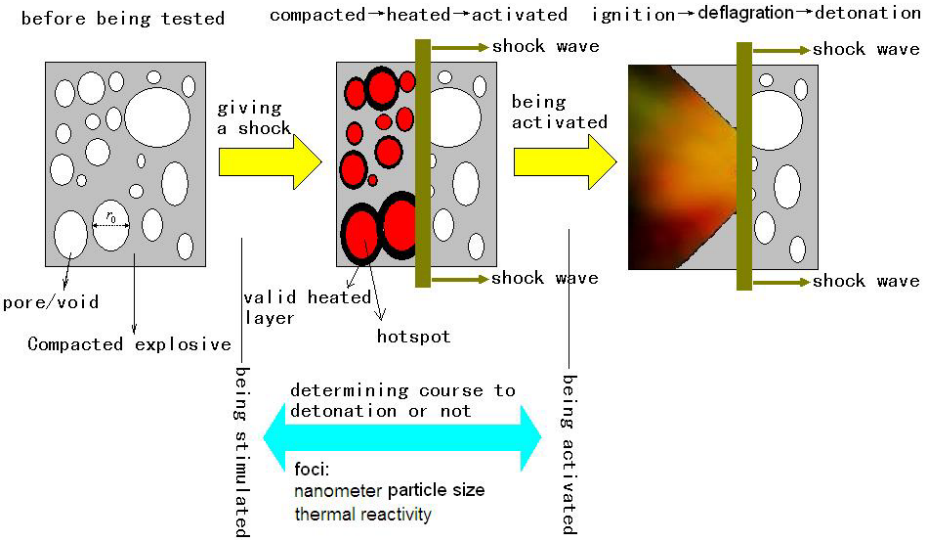

Figure 5. Illustration of shock induced, hotspot formation and growth, in a porous, condensed-phase, explosive-based energetic formulation.

In Partom's theory, if the explosive particles show spherical micron morphology and the charge has a high bulk density, the average pore radius (r_0) is a function of the average size of the explosive particles (d_{50}) and their porosity (Φ) [21]. In Equation 1 it seems that the pore radius in a nanometer RDX charge is significantly smaller than the pore size in a micro RDX charge. After relating the r_0 and d_{50}, the question becomes how large the critical size is. Merzhanov considered that in an explosive charge embedding a chemical heat source, the velocity of the whole heat change is equal to the summation of the rate of heat conduction and the rate of heat release from the chemical source (Equation 2) [22]. Based on this model (Equation 2), the relationship between the critical size (δ_C) and the critical temperature (T_C) was inferred as Equation 3. Substituting the data obtained in our laboratory, we plotted the relationship of δ_C vs T_C in Figure 6. The association of particle size, pore size, critical size, and critical temperature were established, as the r_0 was set to δ_C. It can be deduced that because the particle size of nanometer RDX is essentially smaller than the

size of micro RDX, the critical temperature of nanometer RDX is considerably higher than that of micro RDX. Therefore, when subjected to the same exoteric stimulation, the pores in a micro RDX charge more easily form the effective hot spots that can heat the adjacent explosive particles to decomposition.

$$r_o = 0.5 d_{50} \left(\frac{6\Phi}{\pi} \right)^{\frac{1}{3}} \tag{1}$$

$$C_E \rho_E \frac{\partial T}{\partial t} = \lambda_E \nabla^2 T + QA \exp(-\frac{E_a}{RT}) \tag{2}$$

$$\delta_C = 3.84 T_C \left(\frac{\lambda_E R}{\rho_E Q A E_a} \right)^{\frac{1}{2}} \cdot \exp\left(\frac{E_a}{2RT_C} \right) \cdot \left[\ln \frac{E_a (T_C - T_0)}{RT_C^{\,2}} \right]^{0.6} \tag{3}$$

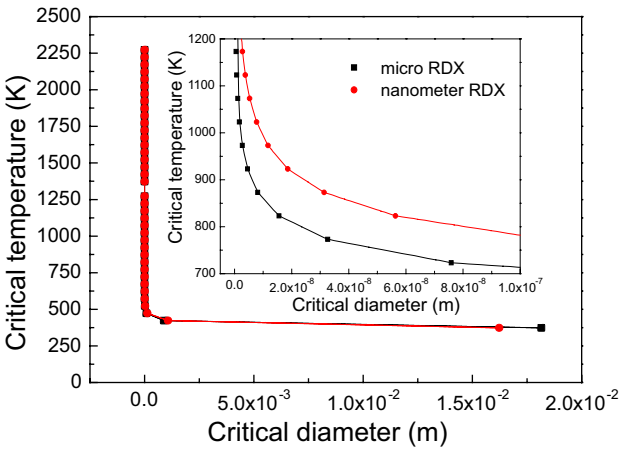

Figure 6. Dependence of critical hot-spot temperature (T_C) on critical hot-spot diameter (δ_C).

Now that the influence of the nanometer particle size has been addressed, another question arises. In the above discussion, we ignored the differences of reactivity between nanometer RDX and micro RDX. If nanometer RDX is far more reactive than micro RDX, the hot spots with lower temperatures (compared to the critical temperature) could also cause thermolysis of energetic particles to occur. In that case, the positive action of the nanometer size would be weakened to a large extent. So what is the reactivity? Obviously, it depends on the decomposition temperature, activation energy, *etc*. In particular, the kinetic properties are more important than the thermodynamic ones. To address

this issue, thermal analysis of micro and nanometer RDX was performed by thermogravimetry at different heating rates, and the TG curves are shown in Figure 7.

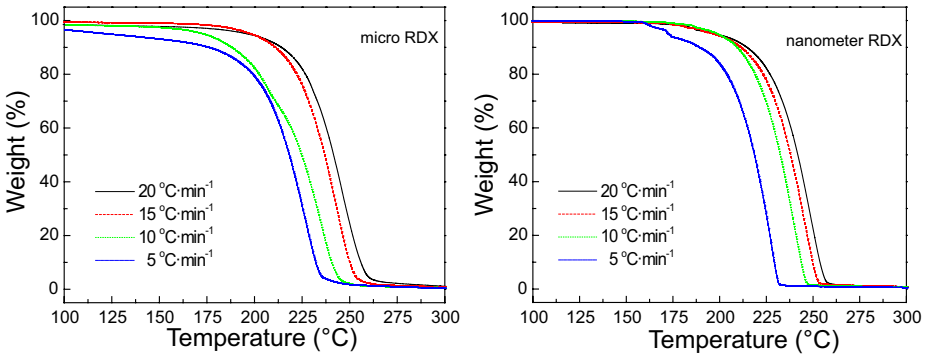

Figure 7. TG curves of samples at different heating rates: (a) for micro RDX; (b) for nanometer RDX.

The plots of dα/dT vs T can be derived from the TG curves [23]. The Kinetic Compensation Effect (Equations 4 and 5) was used to calculate the pre-exponential factor (A_{inv}) and the activation energy (E_{inv}). The specific calculation method refers to Ref. [23]. Equation 7 can be inferred from the base formulation (Equation 6). In Equation 7, $f(\alpha)=m(1-\alpha)^n$. For example, when $m=2$ and $n=0.5$, based on the four heating rates, four plots were fitted in Figure 9 (a for micro RDX, b for nanometer RDX). In each plots, an E_i and A_i can be obtained. By using different $f(\alpha)$ values (*i.e.* different m and n values), many values of E_i and A_i can be calculated. The values of E_i and A_i are listed in Tables 2 and 3. Using Equation 4, plots of $\ln A_i$ *vs.* E_i were fitted and values of a and b were obtained (in Figure 9 and Table 4). Then, using Equation 5, the value of A_{inv} and E_{inv} were obtained, as in Figure 10. For micro RDX, $E_{inv}=168.482$ kJ·mol^{-1} and $A_{inv}=1.087\times10^{17}$ s^{-1}; for nanometer RDX, $E_{inv}=152.658$ kJ·mol^{-1} and $A_{inv}=8.696\times10^{14}$ s^{-1}.

$$\ln A_i = aE_i + b \tag{4}$$

$$b_j = \ln A_{inv} + E_{inv}a_j \tag{5}$$

$$\frac{d\alpha}{dT} = \frac{A}{\beta} f(\alpha)\exp(-\frac{E}{RT}) \tag{6}$$

$$\ln[\frac{d\alpha}{dT}\cdot f^{-1}(\alpha)] = \ln(\frac{A}{\beta}) - \frac{E}{RT} \tag{7}$$

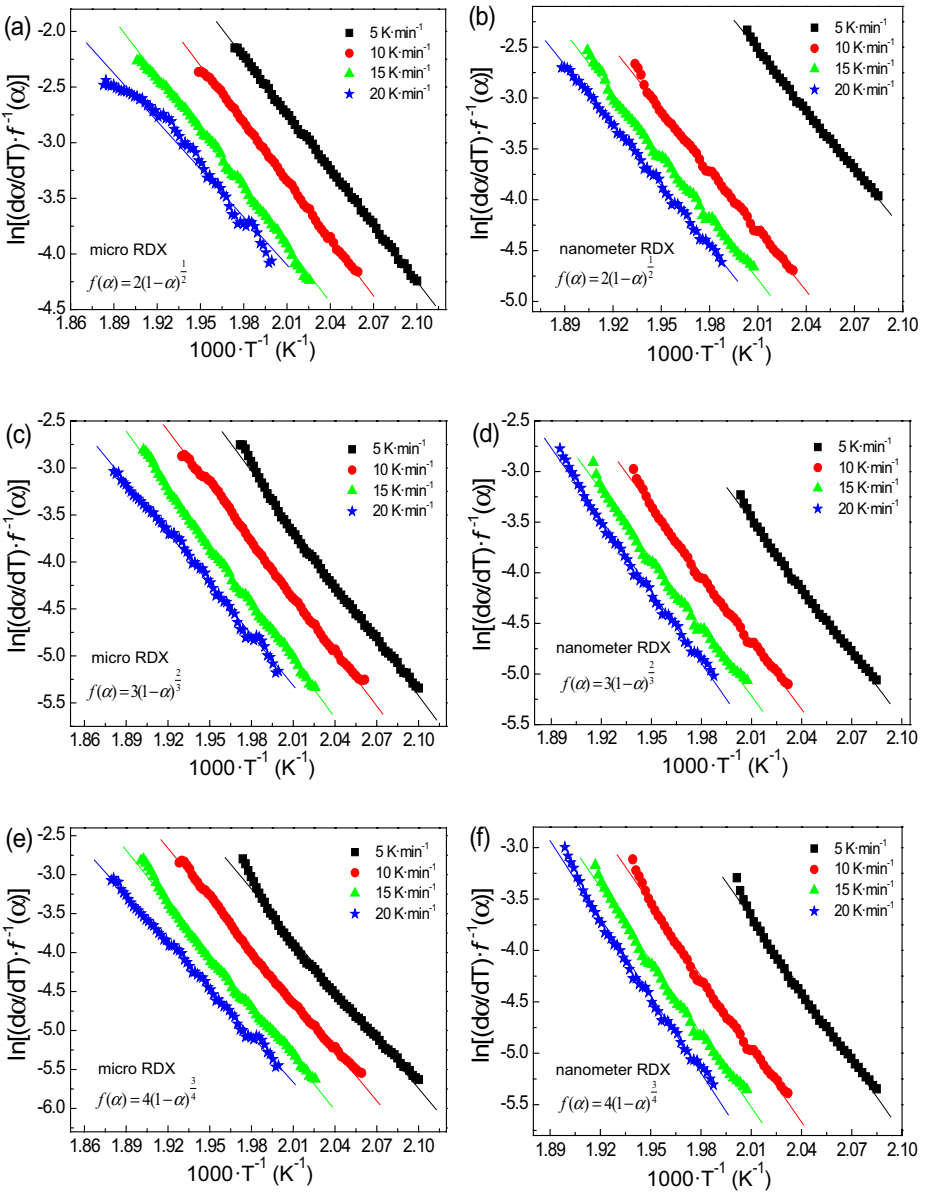

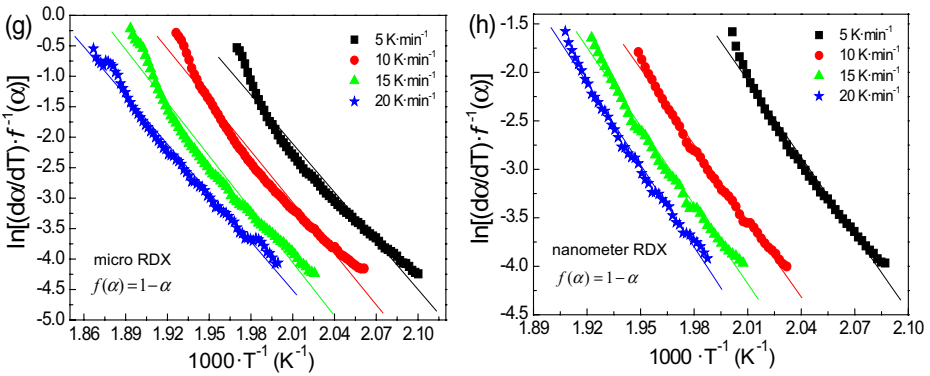

Figure 8. Plots of $\ln[(d\alpha/dT)\cdot f^{-1}(\alpha)]$ *vs.* 1000 T^{-1} for micro and nanometer RDX: (a, b) for micro and nanometer RDX with $f(\alpha)=2(1-\alpha)^{1/2}$; (c, d) for micro and nanometer RDX with $f(\alpha)=3(1-\alpha)^{2/3}$; (e, f) for micro and nanometer RDX with $f(\alpha)=4(1-\alpha)^{3/4}$; (g, h) for micro and nanometer RDX with $f(\alpha)=1-\alpha$.

Table 2. Kinetic parameters for the pyrolysis of micro RDX. *D* is the residual sum of squares of $(d\alpha/dT)_i$ to $k_i(T)[f(\alpha_i)]_\alpha$

β [K·min^{-1}]	E_i [kJ·mol^{-1}]	$A_i\times10^{-16}$ [s^{-1}]	R^2	$D\times10^4$	$f(\alpha)$	Code
5	139.707	0.01513	0.9996	7.286	$2(1-\alpha)^{1/2}$	R_2
10	143.847	0.04483	0.9993	6.063		
15	141.444	0.02096	0.9966	3.397		
20	119.346#	0.0001127#	0.9713	8.578		
Mean	141.666	0.02697	–	–	–	–
S_{dev}	2.079	0.01574	–	–	–	–
5	165.47	3.129	0.9943	3.581	$3(1-\alpha)^{2/3}$	R_3
10	162.40	1.436	0.9981	7.823		
15	169.15	5.524	0.9983	8.154		
20	150.05#	0.05584#	0.9951	2.117		
Mean	165.67	3.363	–	–	–	–
S_{dev}	3.380	2.054	–	–	–	–
5	179.543	78.48	0.9889	5.290	$4(1-\alpha)^{3/4}$	–
10	179.720	74.01	0.9968	1.368		–
15	184.912	184	0.9945	2.123		–
20	166.013#	1.868#	0.9971	1.049		–
Mean	181.392	112.163	–	–	–	–
S_{dev}	3.05	62.253	–	–	–	–

β [K·min^{-1}]	E_i [kJ·mol^{-1}]	$A_i\times10^{-16}$ [s^{-1}]	R^2	$D\times10^4$	$f(\alpha)$	Code
5	221.191	1.02×10^7	0.9679	19.446	1−α	F_1
10	232.849	1.302×10^8	0.9747	16.378		
15	242.299	7.147×10^8	0.9717	20.999		
20	221.502	3.958×10^6	0.9889	6.188		
Mean	229.460	2.148×10^8	–	–	–	–
S_{dev}	10.133	3.385×10^8	–	–	–	–

[#] Abnormal data that were not adopted when calculating the mean value and S_{dev}.

Table 3. Kinetic parameters for the pyrolysis of nanometer RDX. D is the residual sum of squares of $(d\alpha/dT)_i$ to $k_i(T)[f(\alpha_i)]_\alpha$

β [K·min^{-1}]	E_i [kJ·mol^{-1}]	$A_i\times10^{-16}$ [s^{-1}]	R^2	$D\times10^4$	$f(\alpha)$	Code
5	162.872	5.045	0.9984	6.393	$2(1-\alpha)^{1/2}$	R_2
10	165.147	2.967	0.9963	3.818		
15	168.327	5.922	0.9955	2.171		
20	164.551	2.430	0.9982	3.821		
Mean	165.224	4.091	–	–	–	–
S_{dev}	2.282	1.662	–	–	–	–
5	181.32	167.7	0.9958	3.98	$3(1-\alpha)^{2/3}$	R_3
10	184.78	233.5	0.9955	1.34		
15	187.44	389.9	0.9943	8.19		
20	196.58[#]	3212[#]	0.9947	2.87		
Mean	184.51	263.7	–	–	–	–
S_{dev}	3.069	114.137	–	–	–	–
5	193.405	2.549×10^3	0.9919	4.841	$4(1-\alpha)^{3/4}$	–
10	196.463	2.976×10^3	0.9931	1.935		–
15	197.405	3.195×10^3	0.9936	1.393		–
20	208.395[#]	$3.991\times10^{4\#}$	0.9924	5.642		–
Mean	195.758	2.907×10^3	–	–	–	–
S_{dev}	2.0912	0.329×10^3	–	–	–	–
5	219.952	7.742×10^6	0.9856	8.096	1−α	F_1
10	217.360	1.940×10^6	0.9923	4.806		
15	225.041	9.761×10^6	0.9892	3.630		
20	234.534[#]	$8.089\times10^{7\#}$	0.9902	1.831		
Mean	220.784	6.481×10^6	–	–	–	–
S_{dev}	3.908	4.060×10^6	–	–	–	–

[#] Abnormal data that were not adopted when calculating the mean value and S_{dev}.

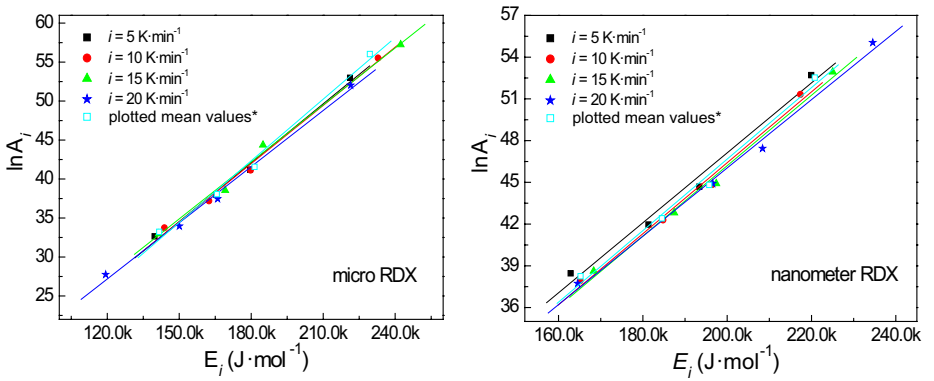

a) b)

Figure 9. Plots of lnA_i *vs.* E_i: (a) for micro RDX; (b) for nanometer RDX. (*These plotted mean values are tabulated in Table 1.)

Table 4. The invariant kinetic parameters for the pyrolysis of micro and nanometer RDX

j / β, [K·min^{-1}]	$^{r}a_j$	$^{r}b_j$	$^{r}R^2$	$^{n}a_j$	$^{n}b_j$	$^{n}R^2$
5	2.517×10^{-4}	−3.221	0.9930	$2.514\times10^{-4\#}$	−3.167$^{\#}$	0.9856
10	2.490×10^{-4}	−2.850	0.9947	2.550×10^{-4}	−4.597	0.9904
15	2.436×10^{-4}	−1.655	0.9938	2.533×10^{-4}	−4.468	0.9927
20	$2.401\times10^{-4\#}$	−1.624$^{\#}$	0.9952	2.455×10^{-4}	−3.057	0.9937
*Values**	2.635×10^{-4}	−5.098	0.9897	2.571×10^{-4}	−4.745	0.9890
Mean	2.496×10^{-4}	−2.890	–	2.525×10^{-4}	−4.007	–
$S_{dev.}$	0.090×10^{-4}	1.424	–	0.044×10^{-4}	0.824	–
	$^{r}E_{inv}$=168.482 kJ·mol^{-1}			$^{n}E_{inv}$=152.658 kJ·mol^{-1}		
	$^{r}A_{inv}=1.087\times10^{17}$ s^{-1}			$^{n}A_{inv}=8.696\times10^{14}$ s^{-1}		

* Values obtained from the plotted mean values presented in Figure 9.

^{r} The parameters for micro RDX. ^{n} The parameters for nanometer RDX.

$^{\#}$ Abnormal data that were not adopted when calculating E_{inv} and A_{inv}.

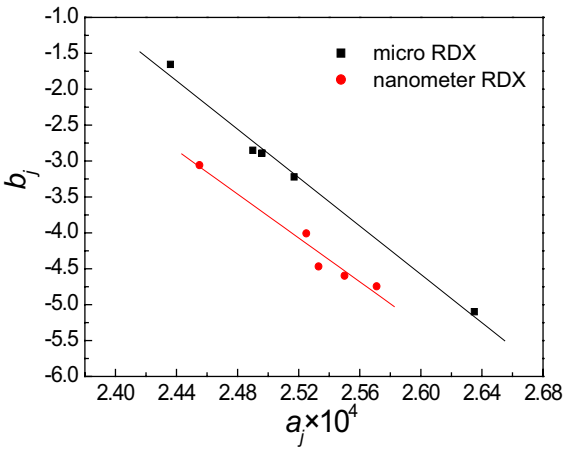

Figure 10. Plots of b_j *vs.* a_j, where a_j and b_j are the coefficients of invariant kinetic parameters tabulated in Table 4, which derives from Equations 4 and 5 ($\ln A_i = aE_i + b$, $b_j = \ln A_{inv} + E_{inv} a_j$).

The results of the kinetic evaluation indicated that the activation energy of nanometer RDX was almost the same as that of micro RDX. This result is certainly different from our expectation that we always considered the decomposition of nanometer RDX should have much lower activation energy than micro RDX. It is generally thought that nanometer energetic materials should be easily ignited, decompose rapidly, and give a violent reaction, *etc*. For example, nanometer thermites and even nanometer AP, increase in thermal reactivity as their particle size falls into the nanometer scale range [24-26]. In our previous studies, the impact and friction sensitivities of nanometer AP were remarkably higher than that of micro AP [26]. This phenomenon cannot be interpreted by any model. However, nitramine explosives behaved differently. Their thermolysis begins with the activation and rupture of the weakest bond in their molecular structure. This activation and rupture are independent of particle size, despite the nanometer scale. Nevertheless, this is a positive indication ensuring the high safety of nanometer nitramines, in that nanometer RDX exhibited similar reactivity to micro RDX. We do not need to consider whether nanometer nitramines are easily decomposed or ignited. Therefore, thermal and kinetic analyses are very important for studying the safety of nanometer sized energetic materials. They are the crucial complement to the detonation physics models. In addition the plastic deformation on an anisotropic slip system is much more localized in RDX than in AP [27].

In fact, many nanometer energetic materials have been fabricated in our

laboratory, such as nanometer RDX, nanometer HMX, nanometer CL-20, nanometer HNS, nanometer AP, nanometerAN, and various nanometer thermites [18, 19, 26, 28-33]. Only nanometer RDX and nanometer HMX exhibit considerably lower sensitivities (impact, friction, and shock sensitivities) than their micron counterparts. Therefore we should not rely excessively on detonation physics models to explain the safety properties of nanometer energetic materials. The high reactivity of nanometer energetic materials cannot be ignored. In conclusion, two foci, *viz*. the nanometer size and the reactivity, determine the sensitivities of nanometer energetic materials.

5 Conclusions

Nanometer RDX was prepared by a mechanical method. After milling, the average size (d_{50}) decreased from 87 μm (micro RDX) to 270 nm (nanometer RDX). Particle agglomeration and the resolution of the PSD instrument (> 0.05 μm) account for $d_{50} > 100$ nm. TEM and SEM images obviously indicated that most of nanometer RDX particles were of the size <100 nm. Its purity was confirmed by XPS and XRD analyses. In this paper, two crucial factors that affect the safety of explosives have been discussed. One is the nanometer size, another is the thermal reactivity. Using Merzhanov's model, we established a relationship of particle size, pore size, and critical temperature. It was concluded that the nanometer particle size led to a very small hot spot size and high critical temperature, which benefited a low sensitivity. The thermal reactivity of nanometer RDX was not ignored in this study. Using the Kinetic Compensation Effect, we calculated the activation energy and pre-exponential factors. It was discovered that the activation energy of nanometer RDX is similar to that of micro RDX. This means that nanometer RDX showed almost the same reactivity as micro RDX, *i.e*. the reactivity was not boosted by the nanometer size. These features ensured the high safety of this nanometer nitramine.

Acknowledgement
This research was supported by the National Natural Science Foundation of China (Grant No. 51206081).

6 References

[1] Hermann Schmid, Coating of Explosives, *J. Hazard. Mater.*, **1986**, *13*(1), 89-101.
[2] Athar J., Ghosh M., Dendage P.S., Nanocomposites: an Ideal Coating Material to Reduce the Sensitivity of Hydrazinium Nitroformate (HNF), *Propellants Explos. Pyrotech.*, **2010**, *35*(2), 153-158.
[3] An C.W., Wang J.Y., Xu W.Z., Preparation and Properties of HMX Coated with a Composite of TNT/Energetic Material, *Propellants Explos. Pyrotech.*, **2010**, *35*(4), 365-372.
[4] Borne L., Patedoye J.-C., Quantitative Characterization of Internal Defects in RDX Crystals, *Propellants Explos. Pyrotech.*, **1999**, *24*(4), 255-259.
[5] Doherty R.M., Relationship between RDX Properties and Sensitivity, *Propellants Explos. Pyrotech.*, **2008**, *33*(1), 4-13.
[6] Li M., Huang M., Kang B., Quality Evaluation of RDX Crystalline Particles by Confined Quasi-static Compression Method, *Propellants Explos. Pyrotech.*, **2007**, *32*(5), 401-405.
[7] Borne L., Mory J., Schlesser F., Reduced Sensitivity RDX (RS-RDX) in Pressed Formulations: Respective Effects of Intra-granular Pores, Extra-granular Pores and Pore Sizes, *Propellants Explos. Pyrotech.*, **2008**, *33*(1), 37-43.
[8] Krober H., Crystallization of Insensitive HMX, *Propellants Explos. Pyrotech.*, **2008**, *33*(1): 33-36.
[9] Song X.L., Li F.S., Dependence of Particle Size and Size Distribution on Mechanical Sensitivity and Thermal Stability of Hexahydro-1,3,5-Trinitro-1,3,5-Triazine, *Defence Sci. J.*, **2009**, *59*(1), 37-42.
[10] Song X.L., Wang Y., An C.W., Dendence of Particle Morphology and Size on the Mechanical Sensitivity and Thermal Stability of Octahydro-1,3,5,7-tetranitro-1,3,5,7-tetrazocine, *J. Hazard. Mater.*, **2008**, *159*(2-3), 222-229.
[11] Czerski H., Proud W.G., Relationship between the Morphology of Granular Cyclotrimethyene-trinitramine and Its Shock Sensitivity, *J. Appl. Phys.*, **2007**, *102*, 1-8.
[12] Field J.E., Hot Spot Ignition Mechanism for Explosive, *Accounts Chem. Res.*, **1992**, *25*, 498-496.
[13] Khasainov B.A., Borisov A.A., Ermolaev B.S., Two-phase Visco-plastic Model of Shock Initiation of Detonation in High Density Pressed Explosives, *7th Symp. Int. on Detonation*, Annapolis, **1981**, 435-447.
[14] Partom Y., Aiod Collapse Model for Shock Initiation, *7th Symp. Int. on Detonation*, Annapolis, **1981**, 506-516.
[15] Politzer P., Lane P., Energetics of Ammonium Perchlorate Decomposition Steps, *J. Mol. Struct.: THEOCHEM*, **1998**, *454*(2-3), 229-235.
[16] Boldyrev V.V., Thermal Decomposition of Ammonium Perchlorate, *Thermochim. Acta*, **2006**, *443*(1), 1-36.
[17] Yuan Y., Jiang W., Wang Y.J., Hydrothermal Preparation of Fe_2O_3/Graphene Nanocomposite and its Enhanced Catalytic Activity on the Thermal Decomposition

of Ammonium Perchlorate, *Appl. Surf. Sci.*, **2014**, *303*(1), 354-359.
[18] Wang Y., Jiang W., Song D., A Feature on Ensuring Safety of Superfine Explosives: the Similar Thermolysis Characteristics Between Micro and Nano Nitroamines, *J. Therm. Anal. Calorim.*, **2013**, *111*(1), 85-92.
[19] Wang Y., Jiang W., Song X.L., Insensitive HMX (Octahydro-1,3,5,7-Tetranitro-1,3,5,7-tetrazocine) Nanocrystals Fabricated by High-yield, Low-cost Mechanical Milling, *Cent. Eur. J. Energ. Mater.*, **2013**, *10*(2), 3-15.
[20] Moulard H., Particular Aspect of the Explosive Particle Size Effect on Shock Sensitivity of Cast Formulations, *9th Int. Detonation Symp.*, Portland, **1989**, 25-38.
[21] Partom Y., A Void Collapse Model for Shock Initiation, *7th Symp. Int. on Detonation*, Annapolis, **1981**, 6-16.
[22] Merzhanov A.G., Barzikin V.V., Gontkovskaya V.T., The Problem of Hot-spot Thermal Explosion, *Doklady AN SSSR*, **1963**, *148*, 380-391.
[23] Vyazovkin S., Burnham A.K., Criado J.M., ICTAC Kinetics Committee Recommendations for Performing Kinetic Computations on Thermal Analysis Data, *Thermochim. Acta*, **2011**, *520*, 1-19.
[24] Kaplowitz D.A., Jian G.Q., Gaskell K., Synthesis and Reactive Properties of Iron Oxide-coated Nanoaluminum, *J. Energ. Mater.*, **2014**, *32*(2), 95-105.
[25] Russell R., Bless S., Pantoya M., Impact-driven Thermite Reactions with Iodine Pentoxide and Silver Oxide, *J. Energ. Mater.*, **2011**, *29*(2), 175-192.
[26] Song X.L., Li F.S., Zhang J.L., Preparation, Mechanical Sensitivity and Thermal Decomposition of AP/Fe_2O_3 Nanocomposite, *J. Solid Rocket Technol.*, **2009**, *32*(3), 306-309.
[27] Armstrong R.W., Bardenhagen S.G., Elban W.L., Deformation-induced Hot-spot Consequences of AP and RDX Crystal Hardness Measurements, *Int. J. Energ. Mater. Chem. Propul.*, **2012**, *11*(5), 413-425.
[28] Wang Y., Song X.L., Song D., A Versatile Methodology Using Sol-gel, Supercritical Extraction, and Etching to Fabricate a Nitramine Explosive: Nanometer HNIW, *J. Energ. Mater.*, **2013**, *31*(1), 49-59.
[29] Guo X.D., Ouyang G., Liu J., Massive Preparation of Reduced-sensitivity Nano CL-20 and Its Characterization, *J. Energ. Mater*., **2014**, *33*(1), 24-33.
[30] Huang H., Wang J.Y., Xu W.Z., Effect of Habit Modifiers on Morphology and Properties of Nano-HNS Explosive in Prefilming Twin-fluid Nozzle-assisted Precipitation, *Propellants Explos. Pyrotech.*, **2009**, *34*(1), 78-83.
[31] Wang Y., Song X.L., Jiang W., Mechanism Investigation for Thermite Reactions of Aluminum/Iron-Oxide Nanocomposites Based on Residues Analysis, *Trans. Nonferrous Met. Soc. China*, **2014**, *24*(1), 263-270.
[32] Wang Y., Jiang W., Zhang X.F., Energy Release Characteristics of Impact-initiated Energetic Aluminum-Magnesium Mechanical Alloy Particles with Nanometer-scale Structure, *Thermochim. Acta*, **2011**, *512*(1-2), 233-239.
[33] Shi X.F., Wang J.Y., Li X.D., Preparation and Characterization of HMX/Estane Nanocomposites, *Cent. Eur. J. Energ. Mater.*, **2014**, *11*(3), 433-442.